



A prediction study for the behaviour of fuel cell membrane subjected to hygro and thermal stresses in running PEM fuel cell

Maher A.R. Sadiq Al-Baghdadi

Faculty of Engineering, University of Kufa, Najaf, Iraq.

Abstract

A three-dimensional, multi-phase, non-isothermal computational fluid dynamics model of a proton exchange membrane fuel cell has been used and developed to investigate the hygro and thermal stresses in polymer membrane, which developed during the cell operation due to the changes of temperature and relative humidity. The behaviour of the membrane during operation of a unit cell has been studied and investigated under real cell operating conditions. The results show that the non-uniform distribution of stresses, caused by the temperature gradient in the cell, induces localized bending stresses, which can contribute to delaminating between the membrane and the gas diffusion layers. These stresses in the membrane may explain the occurrence of cracks and pinholes in the membrane under steady-state loading during regular cell operation. The results show that the maximum displacements in membrane for the low, intermediate and high load conditions were 2.58, 2.66, and 2.78 μm respectively.

Copyright © 2016 International Energy and Environment Foundation - All rights reserved.

Keywords: Proton exchange membrane (PEM); Fuel cell; Nafion; Thermal stresses; Plastic deformation; Mechanical behaviour; CFD model.

1. Introduction

The need for improved lifetime of proton exchange membrane (PEM) fuel cells necessitates that the failure mechanisms be clearly understood and life prediction models be developed, so that new designs can be introduced to improve long-term performance. Durability is a complicated phenomenon, linked to the chemical and mechanical interactions of the fuel cell components, i.e. electrocatalysts, membranes, gas diffusion layers, and bipolar plates, under severe environmental conditions, such as elevated temperature and low humidity [1, 2]. In fuel cell systems, failure may occur in several ways such as chemical degradation of the ionomer membrane or mechanical failure in the PEM that results in gradual reduction of ionic conductivity, increase in the total cell resistance, and the reduction of voltage and loss of output power [3]. Mechanical damage in the PEM can appear as through-the-thickness flaws or pinholes in the membrane, or delaminating between the polymer membrane and gas diffusion layers [4]. An operating fuel cell has varying local conditions of temperature, humidity. As a result of in the changes in temperature and moisture, the membrane, GDL and bipolar plates will all experience expansion and contraction. Because of the different thermal expansion and swelling coefficients between these materials, hygro-thermal stresses are introduced into the unit cell during operation. In addition, the non-uniform current and reactant flow distributions in the cell result in non-uniform temperature and moisture content of the cell which could in turn, potentially causing localized increases in the stress

magnitudes, and this leads to mechanical damage, which can appear as through-the-thickness flaws or pinholes in the membrane, or delaminating between the polymer membrane and gas diffusion layers [5]. Therefore, in order to acquire a complete understanding of these damage mechanisms in the membranes, mechanical response under steady-state hygro-thermal stresses should be studied under real cell operation conditions.

The development of physically representative models that allow reliable simulation of the processes under realistic conditions is essential to the development and optimization of fuel cells, improve long-term performance, the introduction of cheaper materials and fabrication techniques, and the design and development of novel architectures. The difficult experimental environment of fuel cell systems has stimulated efforts to develop models that could simulate and predict multi-dimensional coupled transport of reactants, heat and charged species using computational fluid dynamic (CFD) methods. The strength of the CFD numerical approach is in providing detailed insight into the various transport mechanisms and their interaction, and in the possibility of performing parameters sensitivity analyses.

Weber and Newman [6] developed one-dimensional model to study the stresses development in the fuel cell. They showed that hygro-thermal stresses might be an important reason for membrane failure, and the mechanical stresses might be particularly important in systems that are non-isothermal. However, their model is one-dimensional and does not include the effects of material property mismatch among PEM, GDL, and bipolar plates.

Tang et al. [7] studied the hygro and thermal stresses in the fuel cell caused by step-changes of temperature and relative humidity. Influence of membrane thickness was also studied, which shows a less significant effect. However, their model is two-dimensional, where the hygro-thermal stresses are absent in the third direction (flow direction). In addition, a simplified temperature and humidity profile was assumed, (constant temperature for each upper and lower surfaces of the membrane was assumed), with no internal heat generation.

Kusoglu et al. [8] simulated a simplified single fuel cell duty cycle to study the mechanical response of fuel cell membranes subjected to a single hygro-thermal loading cycle. In their two-dimensional model, linear, uncoupled temperature and humidity profile, assuming steady-state conditions, was used for the loading-unloading. Their results show that the use of temperature and humidity dependent material properties in the mechanical modelling of the membranes leads to critical residual stresses after one fuel cell duty cycle. Their results suggest that the in-plane residual tensile stresses developed upon unloading, may lead to the failure of the membranes due to the mechanical fatigue. They also concluded that to acquire a complete understanding of these damage mechanisms in the membranes, mechanical response under continuous hygro-thermal cycles should be studied under real cell operating conditions.

An operating fuel cell has varying local conditions of temperature, humidity, and power generation (and thereby heat generation) across the active area of the fuel cell in three-dimensions. Nevertheless, no models have yet been published to incorporate the effect of hygro-thermal stresses into actual fuel cell models to study the effect of these real conditions on the stresses developed in the membrane.

In this paper a three-dimensional, multi-phase, CFD model of a PEM fuel cell has been used and developed to investigate the behaviour of the membrane during the operation of a unit cell under real cell operating conditions.

2. Model description

The three-dimensional CFD model of a PEM fuel cell that used with the present stress model was developed, validated, and discussed in detail by the current author in his previous work [9]. In brief, the model is based on the computational fluid dynamics method and considers multi-phase, multi-component flow inside the gas flow channels and the porous media of a PEM fuel cell with straight flow channels. The full computational domain consists of cathode and anode gas flow channels, and the membrane electrode assembly as shown in Figure 1. The model accounts for both gas and liquid phase in the same computational domain, and thus allows for the implementation of phase change inside the gas diffusion layers. The model includes the transport of gaseous species, liquid water, protons, energy, and water dissolved in the ion-conducting polymer. Water transport inside the porous gas diffusion layer and catalyst layer is described by two physical mechanisms: viscous drag and capillary pressure forces, and is described by advection within the gas channels. Water transport across the membrane is also described by two physical mechanisms: electro-osmotic drag and diffusion. Water is assumed to be exchanged among three phases; liquid, vapour, and dissolved, and equilibrium among these phases is assumed. This model takes into account convection and diffusion of different species in the channels as well as in the

porous gas diffusion layer, heat transfer in the solids as well as in the gases, and electrochemical reactions. The model reflects the influence of numerous parameters on fuel cell performance including geometry, materials, operating and others to investigate the in situ stresses in polymer membranes. This model has been used and developed (section 3) to investigate the behaviour of polymer membrane under hygro and thermal stresses during the cell operation.

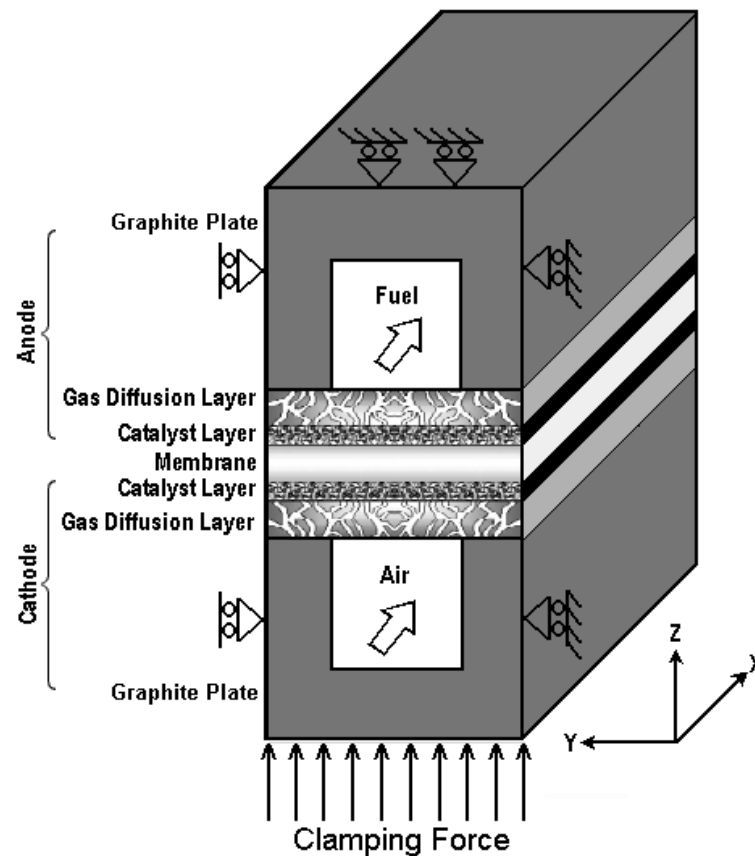


Figure 1. Three-dimensional computational domain.

The governing equations were discretized using a finite-volume method and solved using the multi-physics CFD code. Stringent numerical tests were performed to ensure that the solutions were independent of the grid size. A computational quadratic mesh consisting of a total of 64586 nodes and 350143 meshes was found to provide sufficient spatial resolution (Figure 2). The coupled set of equations was solved iteratively, and the solution was considered to be convergent when the relative error was less than 1.0×10^{-6} in each field between two consecutive iterations.

The solution begins by specifying a desired current density of the cell to use for calculating the inlet flowrates at the anode and cathode sides. An initial guess of the activation overpotential is obtained from the desired current density using the Butler–Volmer equation. Then follows by computing the flow fields for each phase for velocities u , v , w , and pressure P . Once the flow field is obtained, the mass fraction equations are solved for the mass fractions of oxygen, hydrogen, nitrogen, and water. Scalar equations are solved last in the sequence of the transport equations for the temperature field in the cell and potential fields in the gas diffusion layers and the membrane. The local current densities are solved based on the Butler–Volmer equation. After the local current densities are obtained, the local activation overpotentials can be readily calculated from the Butler–Volmer equation. The local activation overpotentials are updated after each global iterative loop. Hooke's law with total strain tensor is solved to determine the stress tensor. Convergence criteria are then performed on each variable and the procedure is repeated until convergence. The properties are updated after each global iterative loop based on the new local gas composition and temperature. Source terms reflect changes in the overall gas phase mass flow due to consumption or production of gas species via reaction and due to mass transfer between water in the vapour phase and water that is in the liquid phase (phase-change). The flow diagram of the algorithm is shown in Figure 3.

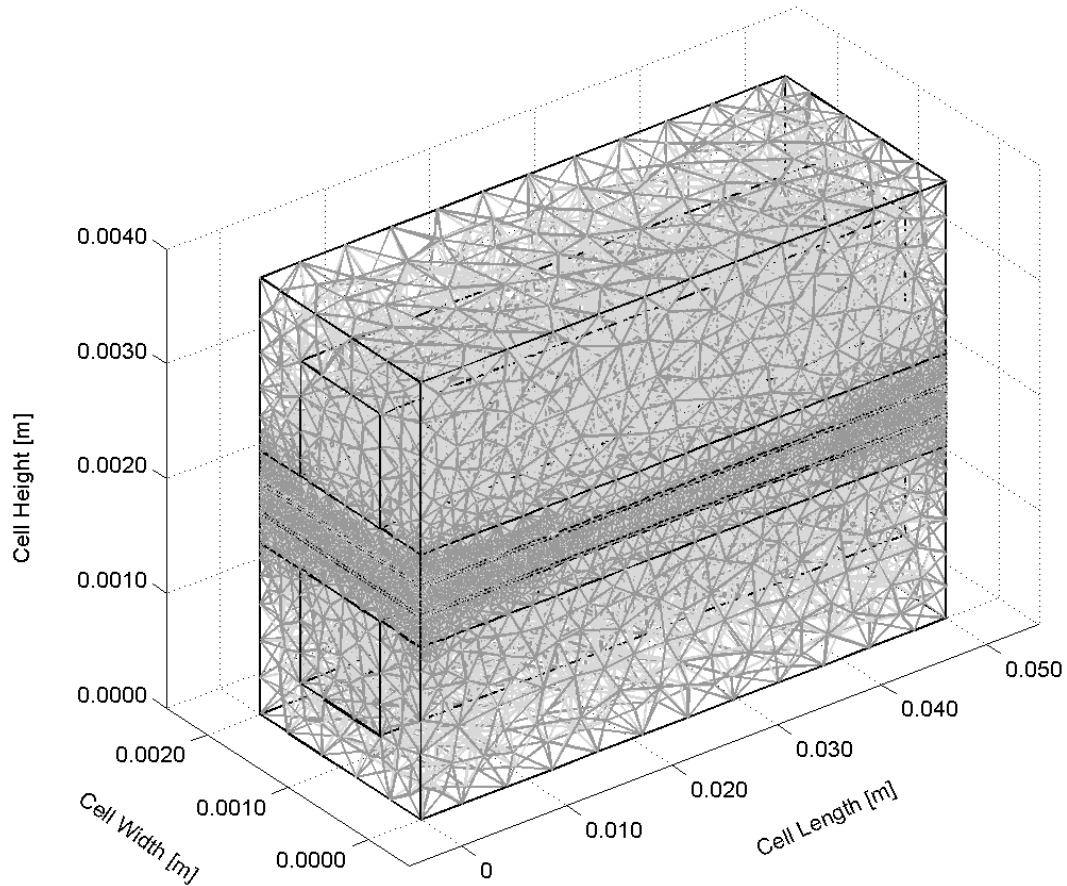


Figure 2. Computational mesh of a PEM fuel cell.

3. Strain tensor in proton exchange membrane

Assuming linear response within the elastic region, the isotropic Hooke's law is used to determine the stress tensor.

$$\sigma = \mathbf{D}\varepsilon \quad (1)$$

where σ is the stress (Pa), ε is the strain, and \mathbf{D} is the constitutive matrix.

Using hygrothermoelasticity theory, the effects of temperature and moisture as well as the mechanical forces on the behaviour of elastic bodies have been addressed. An uncoupled theory is assumed, for which the additional temperature changes brought by the strain are neglected [7, 8]. The total strain tensor in membrane (ε_{mem}) is determined using the following expression;

$$\varepsilon_{mem} = \varepsilon_M + \varepsilon_T + \varepsilon_S \quad (2)$$

where, ε_M is the contribution from the mechanical forces and ε_T , ε_S are the thermal and swelling induced strains, respectively.

The thermal strains resulting from a change in temperature of an unconstrained isotropic volume are given by;

$$\varepsilon_T = \alpha_{mem}(T - T_{Ref}) \quad (3)$$

where α_{mem} is membrane thermal expansion (1/K), and T is local temperature (K).

Similarly, the swelling strains caused by moisture change are given by;

$$\varepsilon_S = \beta_{mem} (\mathfrak{R} - \mathfrak{R}_{Ref}) \quad (4)$$

where β_{mem} is the membrane swelling coefficient tensor due to moisture absorption (1/%), and \mathfrak{R} is relative humidity (%).

The material properties for the fuel cell components used in this model are taken from (DuPont Nafion[®] Data Sheet [10], Tang et al. [7], and Kusoglu et al. [8]) and are listed in Table 1. The geometric and the base case operating conditions are listed in Table 2.

The mechanical boundary conditions are noted in Figure 1. The initial conditions corresponding to zero stress-state are defined; all components of the cell stack are set to reference temperature 20 C, and relative humidity 35% (corresponding to the assembly conditions) [7, 8]. In addition, a constant pressure of (1 MPa) is applied on the surface of lower graphite plate, corresponding to a case where the fuel cell stack is equipped with springs to control the clamping force.

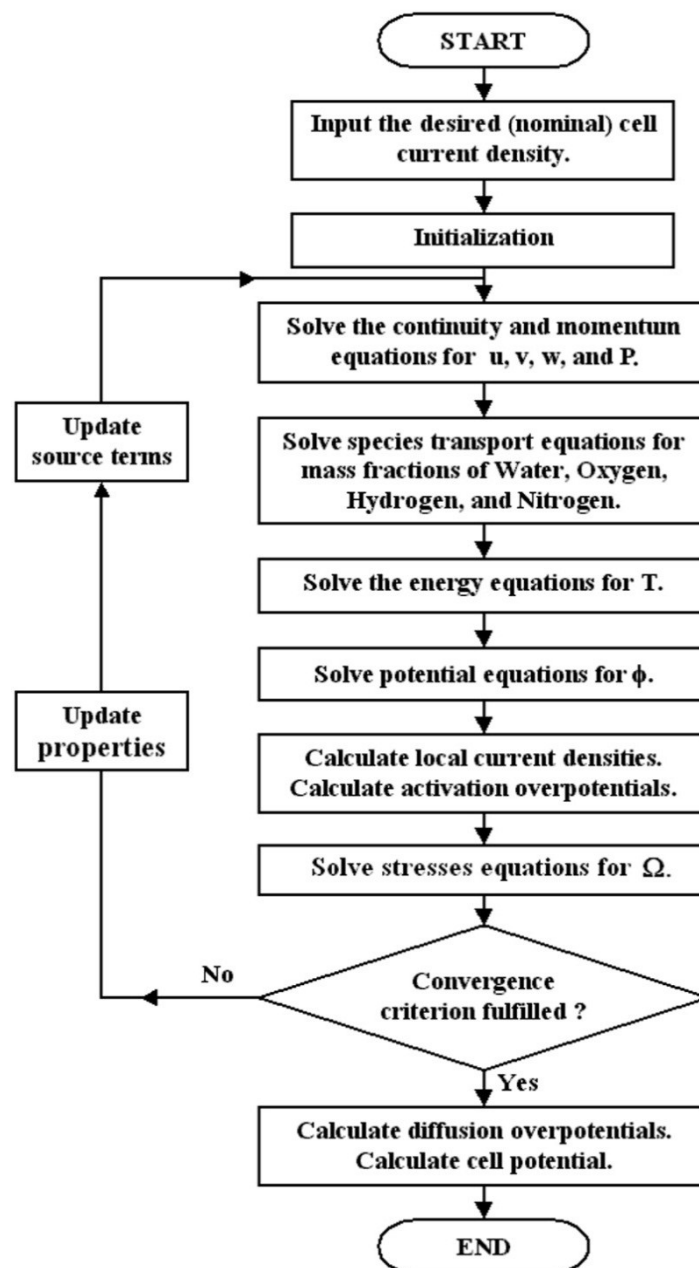


Figure 3. Flow diagram of the solution procedure used.

Table 1. Material properties of the fuel cell components.

Parameter	Symbol	Value	Unit
Electrode thermal conductivity	k_{GDL}	1.3	$W/m.K$
Membrane thermal conductivity	k_{mem}	0.455	$W/m.K$
Bipolar plates thermal conductivity	k_{BP}	95	$W/m.K$
Electrode specific heat capacity	$C_{p,GDL}$	500	$J/kg.K$
Membrane specific heat capacity	$C_{p,mem}$	1050	$J/kg.K$
Bipolar plates specific heat capacity	$C_{p,BP}$	750	$J/kg.K$
Electrode Poisson's ratio	ν_{GDL}	0.25	-
Membrane Poisson's ratio	ν_{mem}	0.25	-
Bipolar plates Poisson's ratio	ν_{BP}	0.25	-
Electrode thermal expansion	α_{GDL}	-0.8e-6	$1/K$
Membrane thermal expansion	α_{mem}	123e-6	$1/K$
Bipolar plates thermal expansion	α_{BP}	5e-6	$1/K$
Electrode Young's modulus	E_{GDL}	1e10	Pa
Membrane Young's modulus	E_{mem}	249e6	Pa
Bipolar plates Young's modulus	E_{BP}	1e10	Pa
Electrode density	ρ_{GDL}	400	kg/m^3
Membrane density	ρ_{mem}	2000	kg/m^3
Bipolar plates density	ρ_{BP}	1800	kg/m^3
Membrane humidity swelling-expansion tensor	β_{mem}	23e-4	$1/\%$

Table 2. Geometrical and operational parameters for base case operating conditions.

Parameter	Symbol	Value	Unit
Channel length	L	0.05	m
Channel width	W	1e-3	m
Channel height	H	1e-3	m
Land area width	W_{land}	1e-3	m
Gas diffusion layer thickness	δ_{GDL}	0.26e-3	m
Wet membrane thickness (Nafion® 117)	δ_{mem}	0.23e-3	m
Catalyst layer thickness	δ_{CL}	0.0287e-3	m
Anode pressure	P_a	3	atm
Cathode pressure	P_c	3	atm
Inlet fuel and air temperature	T_{cell}	353.15	K
Relative humidity of inlet fuel and air (fully humidified conditions)	\mathfrak{R}	100	$\%$
Air stoichiometric flow ratio	ξ_c	2	-
Fuel stoichiometric flow ratio	ξ_a	2	-

4. Results and discussion

The multi-phase model is validated by comparing model results to experimental data provided by Wang et al. and presented in reference [9] in the same conditions of Tables 1 and 2. The importance of phase change to the accurate modelling of fuel cell performance is illustrated. Figure 4 shows the comparison of the polarization curves from the experimental data with the values obtained by the model at different operating fuel cell temperatures. It can be seen that the modelling results compare well with the experimental data. The importance of phase change to the accurate modelling of fuel cell performance is illustrated. Performance curves with and without phase change are also shown in Figure 4 for the base case conditions (on the top right corner of the figure). Comparison of the two curves demonstrates that the effects of liquid water accumulation become apparent even at relatively low values of current density. Furthermore, when liquid water effects are not included in the model, the cell voltage does not exhibit an increasingly steep drop as the cell approaches its limiting current density. This drop off in performance is clearly demonstrated by experimental data, but cannot be accurately modelled without the incorporation of phase change. By including the effects of phase change, the current model is able to more closely simulate performance, especially in the region where mass transport effects begin to dominate.

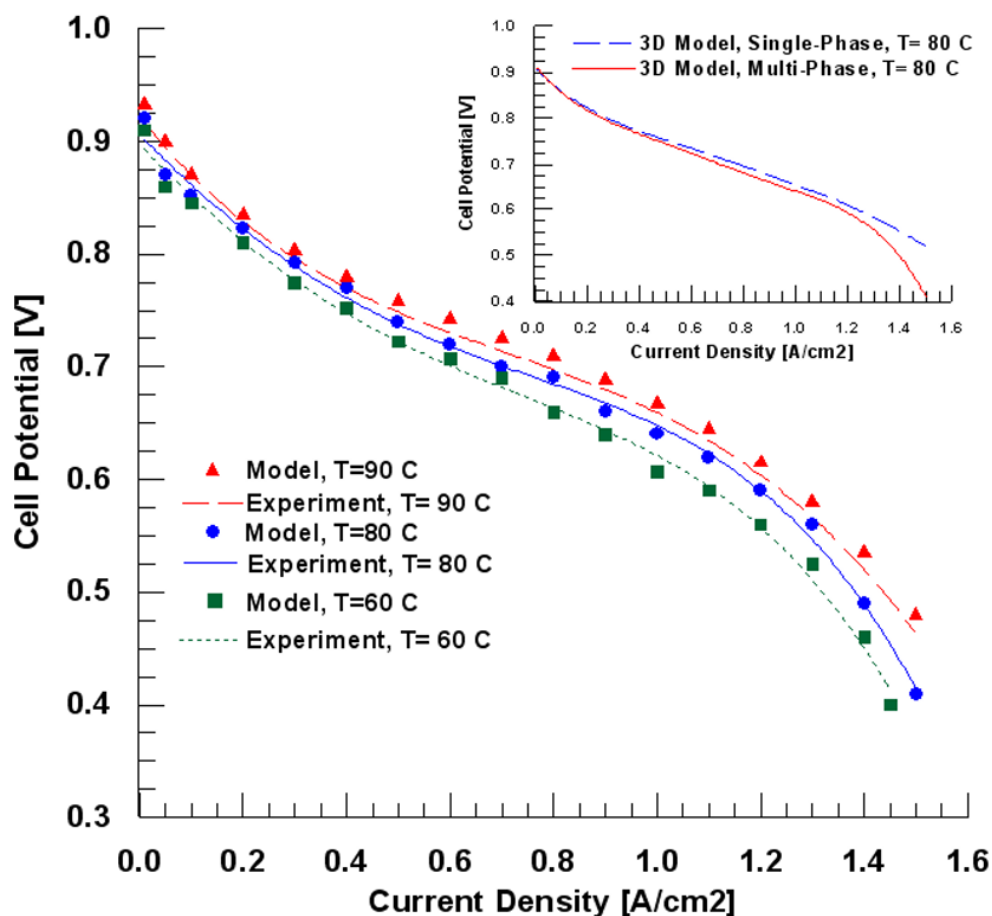


Figure 4. Comparison of the model and the experimental polarization curves.

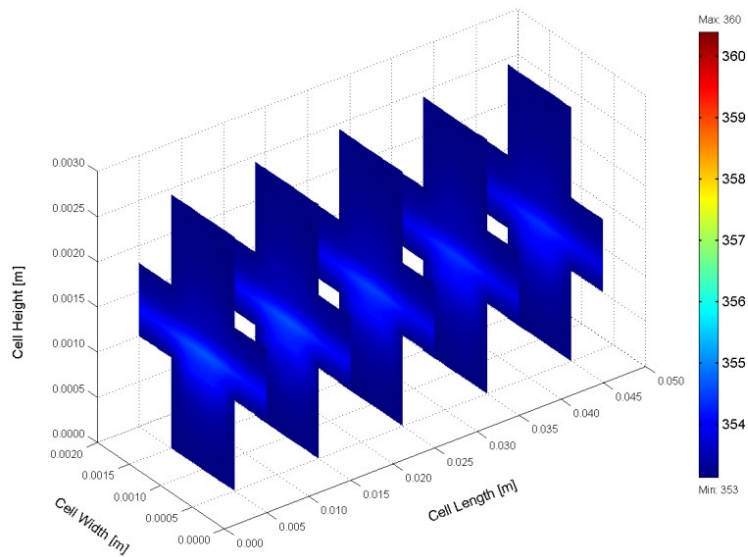
Thermal management is required to remove the heat produced by the electrochemical reaction in order to prevent drying out of the membrane and excessive thermal stresses that may result in rupture of the membrane. The small temperature differential between the fuel cell stack and the operating environment make thermal management a challenging problem in PEM fuel cells. The temperature distribution inside the fuel cell has important effects on nearly all transport phenomena, and knowledge of the magnitude of temperature increases due to irreversibilities might help preventing membrane failure. Temperature distribution for the low, intermediate and high load conditions are demonstrated in Figure 5. In general,

the temperature at the cathode side is higher than at the anode side, due to the reversible and irreversible entropy production. Naturally, the maximum temperature occurs, where the electrochemical activity is highest, which is near the cathode side inlet area. The temperature peak appears in the cathode catalyst layer, implying that major heat generation takes place in this region. In all loading conditions, the distributions of temperature are similar. However, the temperature increase for low load condition of 0.3 A/cm^2 is small, only 1.537 K . This is different for high nominal current density (1.2 A/cm^2). A much larger fraction of the current is being generated near the inlet of the cathode side at the catalyst layer and this leads to a significantly larger amount of heat being generated here. The maximum temperature is more than 7 K above the gas inlet temperature and it occurs inside the cathode catalyst layer.

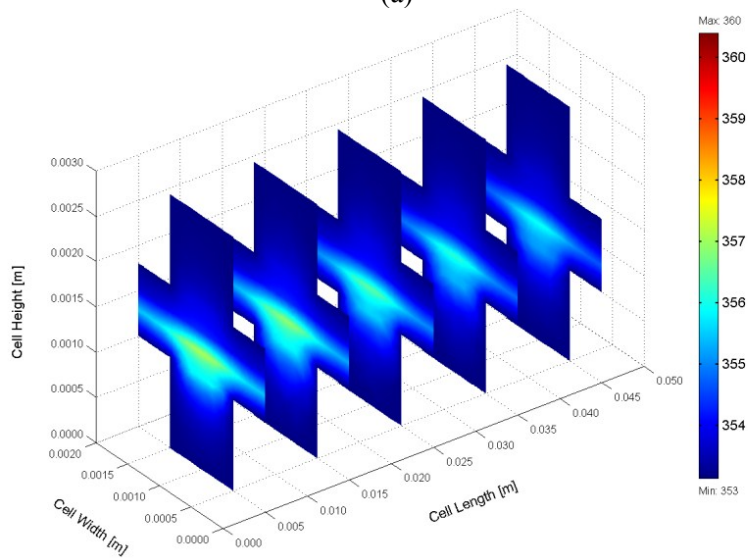
The durability of proton exchange membranes used in fuel cells is a major factor in the operating lifetime of fuel cell systems. The strain distribution that developed during the cell operating can be seen in Figure 6, for three different nominal current densities. It can be seen that the maximum strain occurs, where the temperature is highest, which is near the cathode side inlet area. The maximum strain appears in the lower surface membrane (cathode side), implying that major heat generation takes place near this region. In all loading conditions, the distributions of strains are similar, with higher values under the channel area. It can be seen that the strain profiles correlate with the local temperature, where the temperature is highest in the centre of the channel and coincide with the highest reactant concentrations. However, the maximum strain for low load condition of 0.3 A/cm^2 is 0.012 . This is different for high nominal current density (1.2 A/cm^2). A much larger fraction of the current is being generated near the inlet of the cathode side at the catalyst layer and this leads to a significantly larger amount of heat being generated here. The maximum strain is about 0.013 and it occurs inside the lower surface of the membrane (cathode side).

Figure 7 shows total displacement (contour plots) and deformed shape of the membrane (scale enlarged 300 times) on the y - z plane at $x=10 \text{ mm}$ for three different nominal current densities. The figure illustrates the effect of stresses on the cell membrane. Because of the different thermal expansion and swelling coefficients between gas diffusion layers and membrane materials with non-uniform temperature distributions in the cell during operation, hygro-thermal stresses and deformation are introduced. The non-uniform distribution of strain, caused by the temperature gradient in cell membrane, induces localized bending stresses, which can contribute to delaminating between the membrane and the gas diffusion layers. It can be seen that the total displacement and the degree of the deformation in membrane are directly related to the temperature, and the total displacement profiles correlate with strains. In addition, the deformation that occurs in membrane under the land areas is much smaller than under the channel areas due to the clamping force effect.

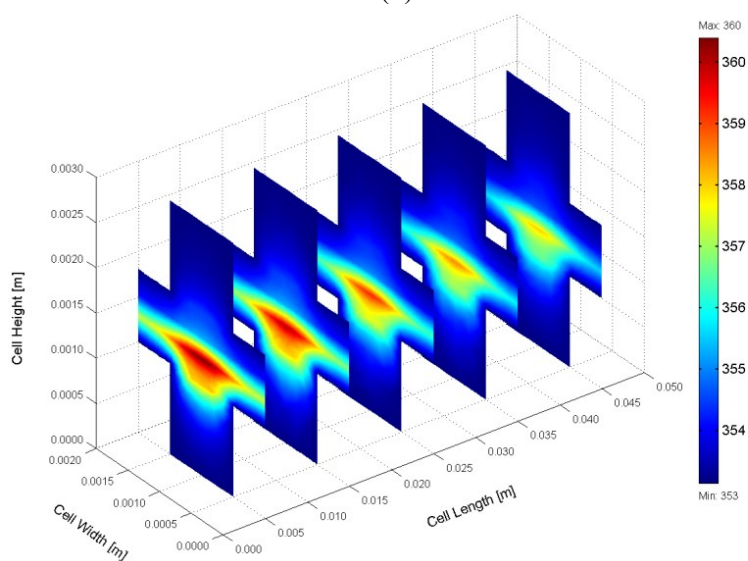
Operating points (cell current density) are based on defining specific system requirements, such as power level, voltage, efficiency, and system weight. Figure 7 shows that the total displacement and the degree of the deformation in membrane are directly related to the increasing of current density, due to increasing of heat generation. This result may explain the occurrence of cracks and pinholes in the membrane under steady-state loading during regular cell operation, especially at high load conditions.



(a)

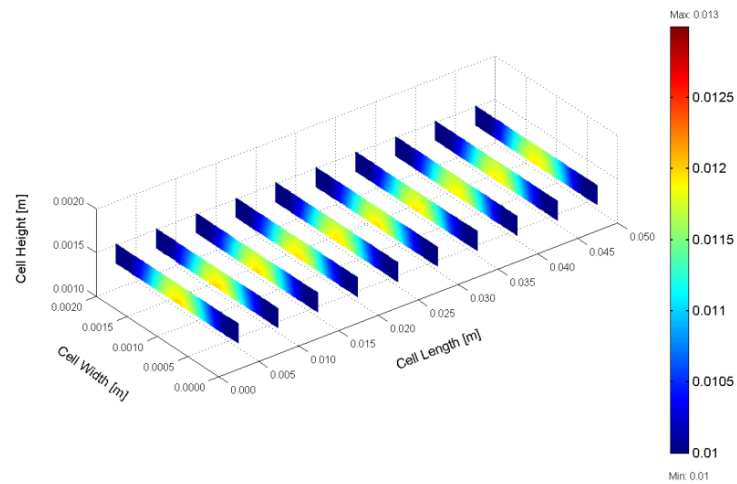


(b)

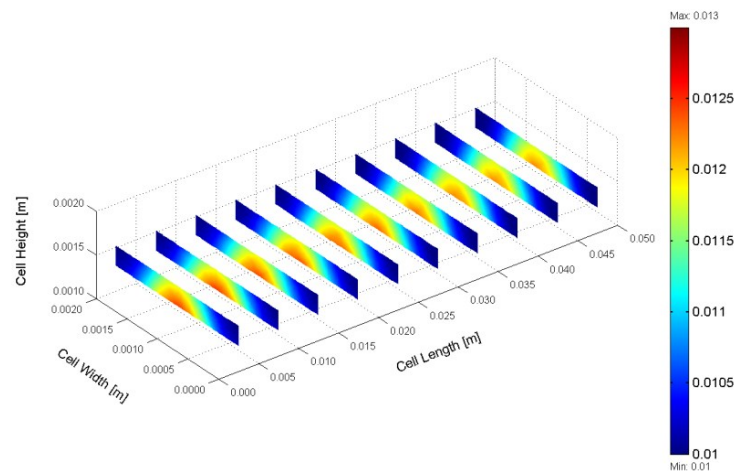


(c)

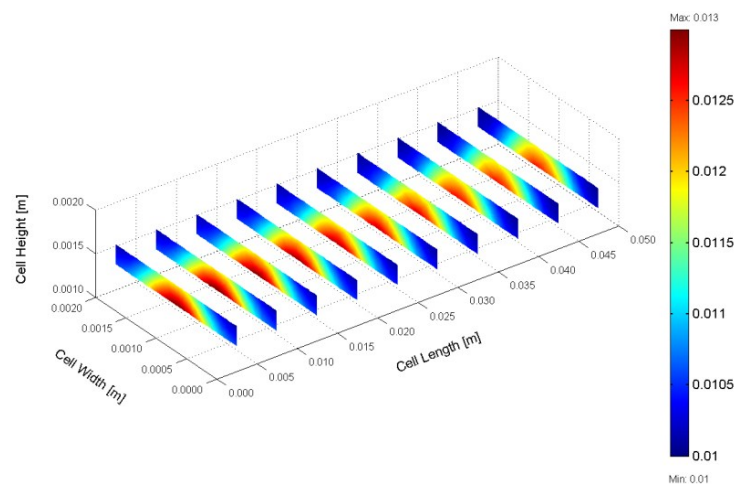
Figure 5. Temperature distribution inside the cell for three different nominal current densities: (a) 0.3 A/cm², (b) 0.7 A/cm², and (c) 1.2 A/cm².



(a)



(b)



(c)

Figure 6. Strain distribution inside the membrane for three different nominal current densities: (a) 0.3 A/cm², (b) 0.7 A/cm², and (c) 1.2 A/cm².

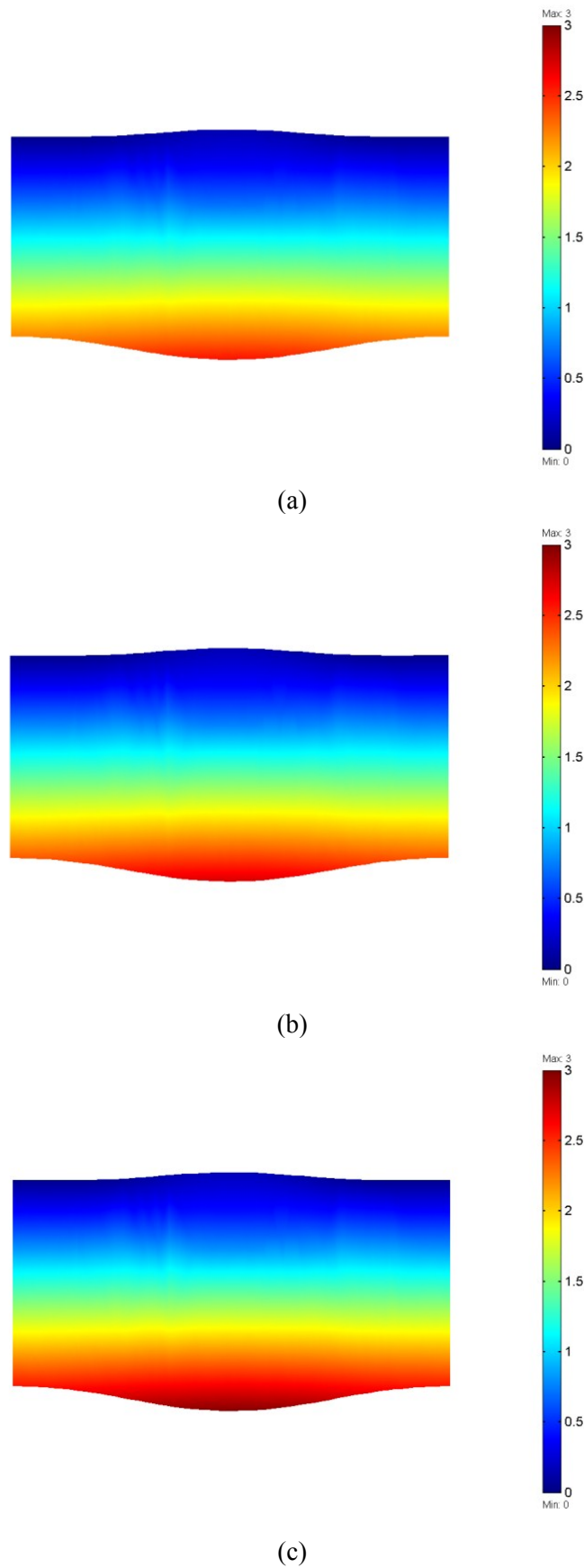


Figure 7. Total displacement (contour (μm)) and deformed shape plot (scale enlarged 300 times) for membrane on the y-z plane at $x=10$ mm for three different nominal current densities: (a) 0.3 A/cm^2 , (b) 0.7 A/cm^2 , and (c) 1.2 A/cm^2 .

5. Conclusion

A full three-dimensional, multi-phase computational fluid dynamics model of a PEM fuel cell with straight flow channels has been used and developed to investigate the hygro-thermal stresses in polymer membrane, which developed during the cell operation due to the changes of temperature and relative humidity. The behaviour of the membrane during operation of a unit cell has been studied and investigated under real cell operating conditions. The results show that the non-uniform distribution of stresses, caused by the temperature gradient in the cell, induces localized bending stresses, which can contribute to delaminating between the membrane and the gas diffusion layers. These stresses in the membrane may explain the occurrence of cracks and pinholes in the membrane under steady-state loading during regular cell operation.

References

- [1] Gode, P., Itonen, J., Strandroth, A., Ericson, H., Lindbergh, G., Paronen, M., Sundholm, F., Sundholm, G., Walsby, N. Membrane Durability in a PEM Fuel Cell Studied Using PVDF Based Radiation Grafted Membranes Fuel Cells. *Fuel Cells* 2003, 3(1-2): 21-27.
- [2] Beuscher, U., Cleghorn, S.J.C., Johnson, W.B. Challenges for PEM fuel cell membranes. *Int. J. Energy Research* 2005, 29(12): 1103-1112.
- [3] Xie, J., Wood, D.L., Wayne, D.M., Zawodzinski, T., Borup, R.L. Durability of Polymer Electrolyte Fuel Cells at High Humidity Conditions. *J. Electrochem. Soc.* 2005, 152(1): A104-A113.
- [4] Stanic, V., Hoberech, M. Mechanical of pin-hole formation in membrane electrode assemblies for PEM fuel cells, in: *Proceedings of the Fourth International Symposium on Proton Conducting Membrane Fuel Cells*, Coral 5, Level 6, Mid Pacific Conference Centre, October 3-8, 2004.
- [5] Tang, Y., Karlsson, A.M., Santare, M.H., Gilbert, M., Cleghorn, S., Johnson, W.B. An experimental investigation of humidity and temperature effects on the mechanical properties of perfluorosulfonic acid membrane. *J. Materials Science and Engineering* 2006, 425(1-2): 297-304.
- [6] Webber, A., Newman, J. A Theoretical Study of Membrane Constraint in Polymer-Electrolyte Fuel Cell. *AIChE J.* 2004, 50(12): 3215–3226.
- [7] Tang, Y., Santare, M.H., Karlsson, A.M., Cleghorn, S., Johnson, W.B. Stresses in Proton Exchange Membranes Due to Hygro-Thermal Loading,, *J. Fuel Cell Sci.&Tech. ASME* 2006, 3(5); 119-124.
- [8] Kusoglu, A., Karlsson, A., Santare, M., Cleghorn, S., Johnson, W. Mechanical response of fuel cell membranes subjected to a hygro-thermal cycle. *J. Power Sources* 2006, 161(2): 987-996.
- [9] Maher A.R. Sadiq Al-Baghdadi. *PEM Fuel Cells - from Single Cell to Stack: Fundamentals, Modeling, Analysis, and Applications*. International Energy and Environment Foundation (IEEF), 2015, ISBN: 9781505885644.
- [10] Product Information, DuPont™ Nafion® PFSA Membranes N-112, NE-1135, N-115, N-117, NE-1110 Perfluorosulfonic Acid Polymer. NAE101, 2005.